Experimental investigation of Hole Boring and Light Sail regimes of RPA by varying laser and target parameters

S. Kar[1,*], K.F. Kakolee[1],M. Cerchez[2], D. Doria[1], A. Macchi[3,4], P. McKenna[5], D. Neely[6], J. Osterholz[2], K. Quinn[1], B. Ramakrishna[1]‡, G. Sarri[1], O. Willi[2], XH Yuan[5]§, M. Zepf[1,7], M. Borghesi[1,8]

[1] Centre for Plasma Physics, School of Mathematics and Physics, Queen's University Belfast, BT7 1NN, UK
[2] Institut für Laser-und Plasmaphysik, Heinrich-Heine-Universität, Düsseldorf, Germany
[3] CNR, Istituto Nazionale di Ottica, Research unit "Adriano Gozzini", via G. Moruzzi 1, 56127, Pisa, Italy
[4] Department of Physics Enrico Fermi, Largo B. Pontecorvo 3, 56127 Pisa, Italy
[5] Department of Physics, SUPA, University of Strathclyde, Glasgow G4 0NG
[6] Central Laser Facility, Rutherford Appleton Laboratory, Didcot, Oxfordshire, OX11 0QX, UK
[7] Helmholtz Institut Jena, D-07743 Jena, Germany
[8] Institute of Physics of the ASCR, ELI-Beamlines Project, Na Slovance 2, 18221 Prague, Czech Republic

E-mail: *s.kar@qub.ac.uk

Abstract.

Temporal evolution of plasma jets from micron-scale thick foils following the interaction of intense (3×10^{20}W cm^{-2}) laser pulses is studied systematically by time resolved optical interferometry. The fluid velocity in the plasma jets is determined by comparing the data with 2D hydrodynamic simulation, which agrees with the expected hole-boring velocity due to the laser radiation pressure. The homogeneity of the plasma density across the jets has been found to be improved substantially when irradiating the laser at circular polarisation compared to linear polarisation. While overdense plasma jets were formed efficiently for micron thick targets, decreasing the target areal density and/or increasing the irradiance on the target have provided indication of transition from the 'Hole Boring (HB)' to the 'Light Sail (LS)' regime of RPA, characterized by the appearance of narrow band spectral features at several MeV/nucleon in proton and carbon spectra.

‡ currently at RRCAT, Indore, India
§ currently at Department of Physics, Shanghai Jiao Tong University, Shanghai 200240, China.

1. Introduction

Significant attention has been paid lately to laser-driven ion acceleration, which potentially offers a compact and cost-effective alternative to conventional sources. While ion beams accelerated by the Target normal sheath acceleration (TNSA) mechanism are characterised by broadband spectrum, modest conversion efficiency and large divergence, Radiation Pressure Acceleration (RPA) is currently attracting a substantial amount of experimental and theoretical attention due to its superior scaling in terms of ion energy and laser-ion conversion efficiency [1].

The ultra-high intensities ($>10^{20}$W cm^{-2}) currently available using Petawatt lasers, offer new opportunities for efficient laser-matter energy coupling. During the interaction of such intense laser pulses with overdense/solid matter, an efficient, directional energy and momentum transfer takes place between the laser pulse and the particles in the target. Electrons are accelerated in the forward direction by the combined effect of the electric and magnetic field of the pulse (e.g. via the $\mathbf{J} \times \mathbf{B}$ mechanism). The directional flow of electrons into the target can lead to efficient ion acceleration via the arising space-charge fields. The pressure (the Ponderomotive force per unit area, or in other words, the flow of delivered momentum per unit area) applied by the intense laser pulse acts as a snowplow, over the duration of the pulse, on the target front surface and launches a dense ion bunch into the target.

For a perfectly reflecting surface, the light pressure, also called Radiation pressure (RP), scales approximately as $660 \times I\lambda^2[\ 10^{18}\text{Wcm}^{-2}\mu\text{m}^2]$ Mbar [2], where I and λ stand for laser intensity and wavelength. This pressure is applied at the target front surface and the ions are driven inward with a velocity (v_f) which, for a semi-infinite target thickness, can be estimated by balancing the momentum flux of the mass flow with the radiation pressure [3, 4]. At the target front surface, the result of such interaction is steepening of the density profile and bending of the critical surface - hence the name hole boring mechanism. 3D particle-in-cell simulations have shown cocoon-like deformation of the target in the extreme case of $I \sim 10^{23}$W cm^{-2} [5]. Although without reaching the dramatic effects observed in this case, the hole-boring velocity at the currently accessible laser intensity (of the order of 10^{20}W cm^{-2}) is high enough for a significant motion of the critical density to take place during the laser pulse duration (a few μm for t $\sim$ 1 ps). When the denting is a significant fraction of the foil thickness, the thrust and density of the ion bunches, attained by the directional momentum transfer from the laser, will lead to a collimated plasma ejection from the rear of thin foil targets, as reported by Kar et. al. [6].

If the target is sufficiently thin, the hole boring front will reach the target rear surface at a time $\tau_{HB} = l/v_f$ (where l is the target thickness) shorter than the incident laser pulse duration (τ_L). As the thickness of the compressed layer becomes comparable to or less than the evanescence length of the Ponderomotive force, the whole layer can be cyclically accelerated with high efficiency for the remainder of the laser pulse duration - which is called Light-Sail(LS) regime of RPA. The acceleration of ions from ultra-thin foils in the LS regime has been recently an area of intense research, with prediction of relativistic ion energies with upcoming laser intensities ([5, 7] and references therein). The mechanism also provides, intrinsically, narrow energy bandwidth ion spectra with high fluxes. Although a pure RPA-LS scenario is hardly possible at the currently available laser parameters, recent experiments have demonstrated the signature of the onset of radiation-dominated ion acceleration [7, 8], which offers high promise for further progress in the near future. This will require

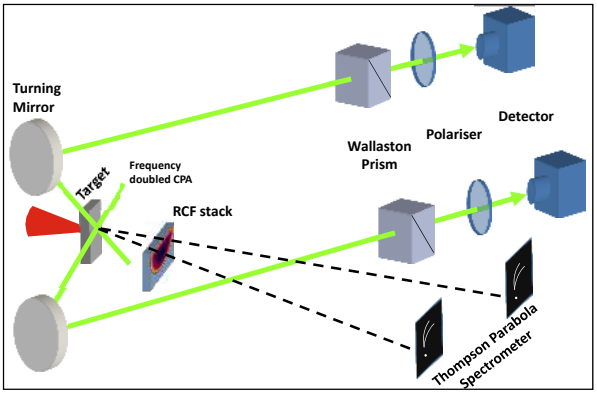

Figure 1. Schematic of the experimental setup, which shows the layouts (not to scale) for the double interferometer setup, ion spectrometers and RCF stack.

addressing a number of challenges, particularly in the Light Sail regime, which employs ultrathin foils, requiring a stringent control on the pulse contrast. Stabilizing the acceleration phase against disruptive transverse instabilities [1] is also challenging, with a number of possible approaches suggested in the literature [1]. Hole Boring is less prone to these problems and can also lead to high ion energies, provided the intensity is high enough or a suitably low target density is available [1, 3].

While ion acceleration in the RP driven HB [6] and LS [7] regimes have been independently reported in separate articles by our group, in this paper we discuss, in addition to a systematic characterisation of HB driven plasma jets (section 3), the transition from HB to LS regimes by reducing the target thickness for the same laser parameters. While plasma jets with velocity corresponding to moderate (sub-MeV) ion energies were formed efficiently for micron thick targets, decreasing the target areal density has led to the appearance of narrow band spectral features at several MeV/nucleon in proton and carbon spectra (section 4), which can be interpreted as a signature of the emergence of the LS regime. In the last section (section 5) we have reported the effect of laser polarisation observed in the HB-regime. The homogeneity of the jet density profile has been found to be improved substantially by irradiating the target at circular polarisation compared to linear polarisation, which is an indication of quasi-static push and reduced electron heating for circular polarisation.

2. Experimental Setup

The data reported in this article has been obtained from an experimental campaign [7] employing the Vulcan Petawatt laser of the Rutherford Appleton laboratory, STFC, UK. A schematic of the experimental setup is shown in the Fig. 1. The chirped pulse amplified (CPA) Vulcan Petawatt laser was focussed on the target by using a f/3 off-axis parabola, delivering a peak intensity of $\sim 3 \times 10^{20}$W cm^{-2} on that target. A single plasma mirror was used before the target in order to suppress the prepulses and amplified spontaneous emission of the laser. Laser polarisation on target was varied from linear to circular by employing a zero-order quarter wave plate in the beam. Targets of various materials and thicknesses were used in this experiment.

On every shot the plasma outflow from the target was characterised at two

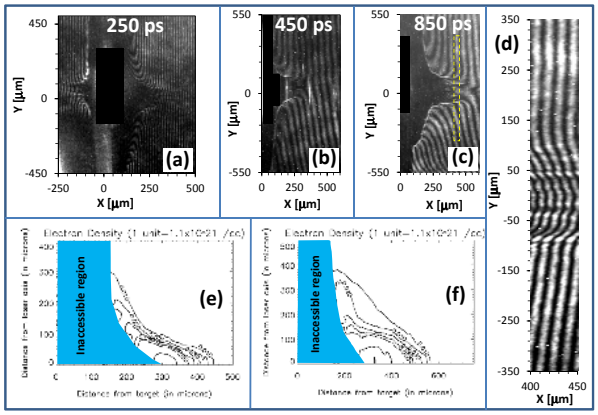

Figure 2. (a)-(c) Raw interferograms obtained in the experiment showing the plasma expansion at three different times after the interaction with 1 μm Cu target. In the images the laser was incident on the target from the left side. **(d)** shows a zoomed-in view of a small part of (c), as marked by the yellow dotted line. **(e)** and **(f)** show the plasma density contour plots at the rear side of the target, obtained from the interferograms shown in (a) and (c) respectively.

different times by deploying two independent transverse Nomarsky interferometer [9] channels. The probe beam used in this setup was created by frequency doubling a very small portion of the main CPA pulse. The second harmonic probe beam was then split into two parts and projected on to the target, transverse to the target plane, from two different angles as shown in the fig. 1. The time of arrival of each beam on the target was controlled by delaying their path lengths independently with respect to the arrival of the main CPA pulse on target. The two interferometric snapshots (with a few μm spatial resolution and ps time resolution) of the plasma jets were recorded by 12 bit dynamic range CCD cameras. Ion spectra produced by the interaction were diagnosed by two Thompson parabola (TP) spectrometers as shown in Fig. 1 (TP1 along the laser axis and TP2 at 13 ± 2 degrees off axis). The energy-resolved spatial profile of the bottom half of the proton beam was recorded by stacks of radiochromic films (RCF). The BAS-TR image plate detectors used in the TPs were cross-calibrated with CR39 solid state nuclear track detectors [10].

3. Formation of collimated plasma jets from micron thick targets

Varying the time delay between the transverse probe and the interaction CPA, the temporal evolution of the plasma jets ejected from the rear side of the targets was observed from ∼100 ps to ∼1.1 ns after the interaction. Fig. 2 (a)-(c) shows the interferograms obtained at three different probing times (where the snapshots in (a) and (c) were taken in the same shot) for the case of 1 μm Cu target irradiated at an intensity of $\sim 3 \times 10^{20}$ W cm^{-2} at linear polarisation. The region where no fringes were observed in the interferograms corresponds to the shadow of the target, typically having a small amount of transverse tilt. Nevertheless, the strong second harmonic self-emission (obscured in the images in order to improve the visibility) from the target enabled locating the interaction point within the shadow. Where a small plasma bulging out from the rear side of the foil was observed at the early probing times, the

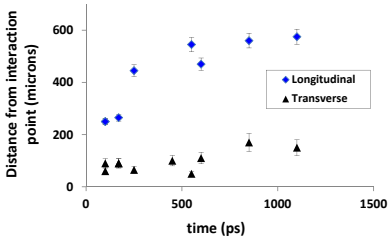

Figure 3. Longitudinal and transverse expansion of iso-density surfaces, of 0.01 times the critical plasma density ($1.1 \times 10^{21}/cc$), in the plasma jets obtained at different probing times. The points shown in the graph are taken from a number of shots (similar to that shown in the fig 2) obtained for 1 μm thick Cu target at linear polarisation. The longitudinal expansion is measured along the laser axis and the transverse expansion is measured just after the shadow of the target.

plasma was observed to expand in a highly collimated fashion over a period of time of the order of ns, as shown in fig 2(a)-(c). The shape of the expanding plasma jets can be seen in the interferograms by following the fringe shifts, which occur due to the change in the refractive index, due to the presence of the plasma. Since the fringe shift in a given region is commensurate to the local plasma density, an abrupt shift in fringe pattern corresponds to an abrupt change in the plasma density. Therefore, as shown in fig. 2(d) (a zoomed view of a small section of the late time plasma jet shown in the fig. 2(c)) one can clearly infer the boundaries of the expanding plasma, which indicates the degree of collimation of the jets.

In order to obtain the plasma density profile from the interferograms, each snapshot was analysed, first by inverting the interferograms into phase maps, followed by Abel inversion of the phase maps assuming a cylindrical symmetry [11]. Fig. 2 (e) and (f) show the plasma density profiles at the target rear surface obtained from the interferograms shown in fig. 2(a) and (c). One can clearly see the significant difference between the longitudinal and transverse extents of the plasma jets, as well as the steep density gradients at their periphery.

The plasma density profile obtained at different times (from $\sim$100 ps to $\sim$1.1 ns after the interaction of CPA) enabled mapping of its expansion profile along the longitudinal (laser axis) and the transverse directions. For example, fig. 3 shows the position of the $0.01n_c$ (where n_c stands for critical plasma density) iso-density surface of the plasma jets at different times. One can clearly see a difference in the jet expansion behaviour along the two orthogonal directions. It is to be noted that the velocity at which an iso-density surface expands over time corresponds to a "phase" velocity of the plasma density, rather than the fluid velocity of the plasma jets. One can clearly see from the fig. 3 that during the early time of expansion (up to several hundreds of ps after the interaction), the density phase velocity is significantly higher along the laser axis compared to that in the transverse direction, which indicates that the plasma jet expands with a fluid velocity predominantly along the laser axis - most likely due to the directional momentum transfer from the laser to the plasma via the radiation pressure.

In order to substantiate the role of the laser radiation pressure, which provides the directional thrust to the plasma jets, the fluid velocity was obtained by modelling

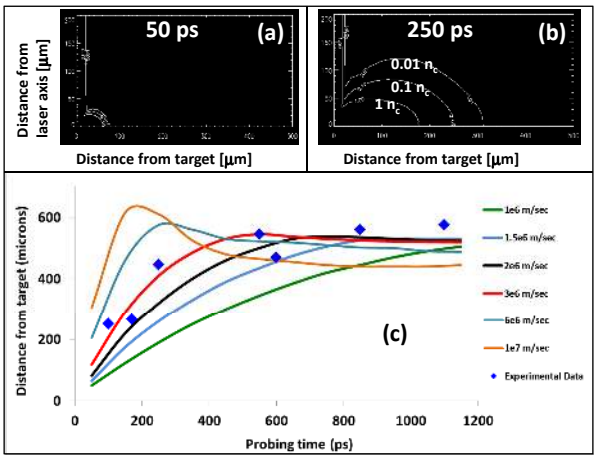

Figure 4. **(a)** and **(b)** shows a typical plasma jet expansion profiles obtained from 2D hydrodynamic simulations as described in the text. In this case the electron and ion temperatures were $\sim$ 50 eV and the mesh velocity was $1.5 \times 10^6 m/sec$. **(c)** shows the simulated longitudinal expansion profiles of $0.01 n_c$ iso-density surface, obtained for different longitudinal mesh velocities, overlaying the experimental data shown in the fig. 3.

the jet expansion using the 2D hydro-code POLLUX [12]. The simulation box was set up in cylindrical symmetry with a fine grid spacing of 1 μm along both the radial and longitudinal axes. The target was modelled as a fully ionised plasma slab of a given thickness and density, corresponding to the target used in the experiment. In order to simulate the jet expansion, a small region of the target close to the laser axis was initialised with given electron and ion temperatures, and a given longitudinal 'mesh' velocity. The 'mesh' velocity in the POLLUX simulation corresponds to the fluid velocity of the plasma. Where the electron and ion temperatures contribute towards an isotropic plasma expansion, the longitudinal mesh velocity results in a directional jet like expansion, as shown in the Fig. 4 (a) and (b). For a longitudinal mesh velocity of the order of 10^6m/sec, it has been observed that a target temperature in the range of 10-100 eV has an insignificant effect on the longitudinal expansion profile of the jets. In order to match the longitudinal expansion profile of the plasma jets obtained in the experimental data, a set of simulations were carried out by varying the initial mesh velocity. The simulated longitudinal expansion profile of $0.01 n_c$ iso-contour surface for different mesh velocities are shown in the fig 4(c). One can see from the figure that the density phase velocity during the initial phase of expansion increases with the increase of the mesh velocity (i.e. the fluid velocity), where the decrease in density phase velocity, or even the recession of iso-density surface for very high mesh velocities, is observed at the later stages because of the finite amount of matter in the expanding plasma. Fig. 4(c) shows that the best match to the experimental data is obtained for a fluid velocity of $2 - 3 \times 10^6$ m/s, which is of the order of the HB velocity one estimates (1.06×10^6 m/s) according to the eq. 10 in the ref. [3]. It is to be noted that the density at the target front surface can be effectively lower than the solid density, because of some pre-plasma expansion by the rising edge of the laser pulse, which can produce higher HB velocity than expected. These expansion velocities correspond to ion energies of the order of tens of keV/nucleon for the bulk Cu ions

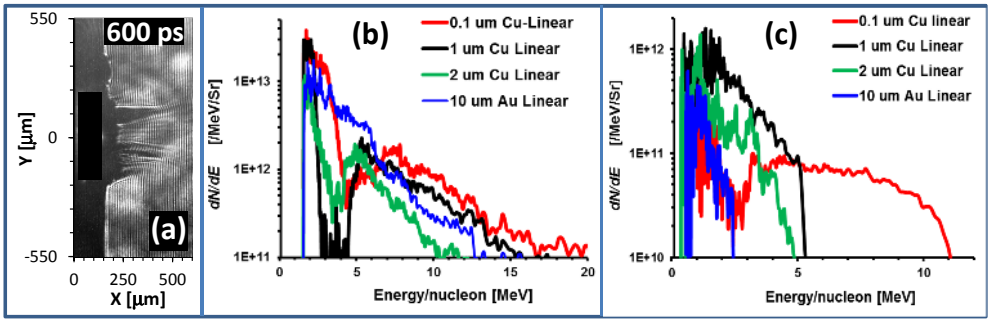

Figure 5. **(a)** Interferogram showing the rear surface plasma profile obtained from a 0.1 μm Cu target irradiated by linearly polarised CPA at peak intensity 3×10^{20}W cm^{-2}. **(b)** and **(c)** show the proton and carbon ion spectra, respectively, obtained along the laser axis (TP1) from targets of various thickness (as mentioned in the legend). The interferogram shown in (a) was taken from the same shot as the 0.1 μm thick Cu target ion spectra shown in (b) and (c).

constituting the jets. During these shots, the TP recorded spectra of higher energy ions (protons and Carbons), accelerated from surface contaminant layers. These spectra have a characteristic exponential profile, and extend to cut-off energies of 10-20 MeV (protons), and a few MeV/nucleon (Carbon) - see for example the spectra for the thicker targets in Fig. 5. The main mechanism accelerating these ions is TNSA for the thicker targets, with features attributable to RPA effects emerging as the target thickness (or areal density) is decreased as discussed in the next section.

4. Transition from HB to LS regime with decrease in target thickness

While dense plasma jets were formed efficiently for micron thick targets, when decreasing the target thickness the jets became less uniform until they were not observed for the thinner targets employed (0.05-0.1 m), where the interferograms displayed features characteristics of exploded foils, as shown in Fig. 5(a). At the same time the MeV proton and ion energy spectra observed by the Thompson parabolas become pronouncedly modulated. Instead of quasi-maxwellian proton spectra typically observed in the case of 10s of micron thick targets, as shown in the fig. 5(b), a breakup in the proton spectrum was observed for targets of 1-2 μm thickness and below. This is the range of thicknesses at which the time τ_{HB} taken by the hole boring front to cross the target becomes comparable to the laser duration τ_L (e.g. using front velocities as inferred from fig.4). As the target areal density was further decreased, the energy at the peak (after the breakup in the spectra) gradually increased. A similar feature also appeared in the carbon ion spectra, as shown in fig. 5(c), showing a pronounced increase in the cutoff energy when $\tau_{HB} \approx \tau_L$, and bunched spectral features for ultra-thin targets. The ion spectra obtained for the ultra-thin targets ($\tau_{HB} \ll \tau_l$) havs been investigated in detail in ref. [7]. In order to interpret this data, one should consider that, for the thin targets, where $\tau_{HB} < \tau_L$, the compressed ion layer from the target front surface reaches the target rear before the end of the pulse, which allows further acceleration of ions in a LS type scenario. For the thinnest target used, τ_{HB} becomes insignificant compared to τ_L [13], and the LS phase is accessed early on during the pulse duration.

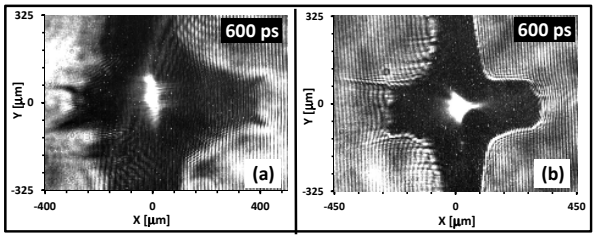

Figure 6. (a) and **(b)** shows the interferograms obtained in case of 1 μm and 5 μm, respectively, Cu targets irradiated by circularly polarised CPA.

One should note that TNSA is also active in these interactions, and contributes to the spectra profiles observed [7, 13]. The strongest RPA effects are observed in the C spectra, for which TNSA acceleration is less efficient, where clear, isolated spectral peaks, are observed for the thinnest targets (see 0.1μm case in fig. 5(c) and fig.2 of [7]). In this data set, the width of the peaks appears to increase for decreasing target areal density, likely associated to an unstable acceleration phase (effects of transverse instability [14], or increased electron heating due to stronger target deformation as the energy of the ions increases). TNSA acts more effectively on the protons due to the higher charge to mass ratio, and therefore the RPA-induced modulations are in this case superimposed on a TNSA spectrum, in the hybrid scenario desecribed in [7, 13].

5. Effect of laser polarisation

Effects of laser polarisation, predicted in many theoretical papers [see [1]], in the RPA regime have been observed previously by Henig et. al. [8], where the experimental data shows a polarisation-dependent modification of the ion spectral profile. In our case, the polarisation dependance was not prominent in the proton and carbon ion spectra obtained for ultra-thin targets [7], possibly due to the relatively long duration (ps) of the interaction CPA. However, the use of circular polarisation showed a significant improvement in the plasma jet density profile obtained for micron-scale thick targets. For example, while the plasma jets from 1μm thick targets irradiated by linearly polarised laser (as shown in the Fig. 2), albeit being dense and well collimated, show a filamentary/non-uniform density profile, a significant improvement in density uniformity has been observed across the jets obtained with circular polarisation, as can be seen in the fig. 6(a) and (b). This may indicate a more uniform and steady Ponderomotive drive for circular polarisation, with significantly less perturbation of the critical density surface during the HB phase, as one could expect due to the absence of the oscillatory component of the $\mathbf{J} \times \mathbf{B}$ force [15, 4].

6. Conclusion

In conclusion, experimental studies investigating the transition from the HB to the LS regime of RPA by reducing the target thickness are presented. The temporal evolution of the collimated plasma jets obtained in the RPA-HB regime (for micron thick targets) has been studied over a time period ranging from 100 ps to 1 ns. Reducing the target thickness down to 0.1 μm resulted in the appearance of narrow-band features in the Carbon spectra, which is a characteristic feature of the RPA-LS

acceleration. Experimental data obtained for circularly polarised CPA interaction indicate more uniform and sustained radiation pressure drive compared to the case of linearly polarised CPA interaction.

7. Acknowledgements

The authors acknowledge funding from EPSRC [EP/J002550/1-Career Acceleration Fellowship held by S. K., EP/E035728, EP/J003832/1 and EP/K022415/1], from projects ELI (Grant No. CZ.1.05/1.1.00/483/02.0061) and OPVK 3 (Grant No. CZ.1.07/2.3.00/20.0279), and from DFG programs TR18 and GK1203. The authors also acknowledge support from the target fabrication group of RAL, STFC, UK.

References

[1] H. Daido, M. Nishiuchi and A.S. Pirozkhov, Rep. Prog. Phys. **75**, 056401 (2012); A. Macchi, M. Borghesi and M. Passoni, Rev. Mod. Phys., **85**, 751 (2013); and references therein.
[2] S. Wilks *et al.*, Phys. Rev. Lett., **69**, 1383 (1992); J. Denavit, Phys. Rev. Lett., **69**, 21 (1992); S. Wilks and W.L. Kruer, IEEE Quant. Elec., **33**, 1954 (1997).
[3] A.P.L. Robinson *et al.*, Plasma Phys. Controll. Fusion, **51**, 024004 (2009)
[4] A. Macchi *et al.*, Phys. Rev. Lett., **94**, 165003 (2005).
[5] T.Zh. Esirkepov *et. al.*, Phys. Rev. Lett., **92**, 175003 (2004).
[6] S. Kar *et al.*, Phys. Rev. Lett., **100**, 225004 (2008);
[7] S. Kar *et al.*, Phys. Rev. Lett., **109**, 185006 (2012);
[8] A. Henig *et al.*, Phys. Rev. Lett. **103**, 245003 (2009).
[9] R. Benattar *et. al.*, Rev. Sci. Instr., **50**, 1583 (1979).
[10] D. Doria *et al.*, Central Laser Facility, RAL, UK, Annual Report 2009/10, p.p. 78.
[11] L.A. Gizzi *et. al.*, Phys. Rev. E, **49**, 5628 (1994).
[12] G.J. Pert, J. Comp. Phys., **43(1)**, 111 (1981).
[13] B. Qiao *et al.*, Phys. Rev. Lett., **108**, 115002 (2012)
[14] F. Pegoraro and S.V. Bulanov, Phys. Rev. Lett. **99**, 065002 (2007).
[15] O. Klimo *et al.*, Phys. Rev. Sp. Topics - Acc. and Beams, **11**, 031301 (2008)